Structure and microwave dielectric properties of $BaLa_4Ti_4O_{15}$

Structure and microwave dielectric properties of BaLa$_4$Ti$_4$O$_{15}$

H Zheng, D I Woodward[1], L Gillie and I M Reaney

Department of Engineering Materials, University of Sheffield, Sheffield S1 3JD, UK

Abstract

BaLa$_4$Ti$_4$O$_{15}$ (BLT) is a compound with a Ti-deficient, layered perovskite-related structure. Dense BLT ceramics have been produced and their crystal structures and microstructures are investigated. The average macroscopic structure of BLT powder is considered to be hexagonal with space group $P\bar{3}c1$, but there is some evidence in high-order x-ray diffraction peaks of asymmetry. Energy-dispersive x-ray analysis and Raman spectroscopy have illustrated that there is a heterogeneous distribution of constituent cations which may induce asymmetry as a result of the presence of two hexagonal phases of slightly different lattice parameter. Despite this inhomogeneity, BLT exhibits a microwave quality factor (Qf) of ∼44 000 GHz, a relative permittivity (ε_r) of ∼45, and a temperature coefficient of resonant frequency (τ_f) of −2 ppm °C^{-1}. In addition, anisotropy in the properties of the ceramic has been observed, with ε_r found to be larger when measured normal to the pressing direction.

1. Introduction

Some ceramics within the BaO–Ln$_2$O$_3$–TiO$_2$ system (where Ln = rare earth) have high permittivities (ε_r), high quality factors Q (low dielectric losses), and low temperature coefficients of resonant frequency (τ_f) and are suitable for microwave applications [1–3]. Recently, high Q values have been reported for materials in the BaTiO$_3$–La$_4$Ti$_3$O$_{12}$ pseudo-binary system [4, 5]. All the compounds in this system belong to the homologous series A$_n$B$_{n-1}$O$_{3n}$ ($n \geqslant 3$) of B-site cation-deficient perovskite-related phases. Their crystal structures are derived from perovskite by the periodic introduction of intrinsic stacking faults in the cubic close packing of AO$_3$ mixed layers. In these structures, slabs of normal cubic perovskite are intergrown with hexagonal close-packed regions of the type found in the hexagonal perovskite BaNiO$_3$ [6]. The change in composition from the ideal perovskite ABO$_3$ is brought about by layers of empty octahedra in the centre of the hexagonal slabs. For a given composition A$_n$B$_{n-1}$O$_{3n}$ ($n \geqslant 3$), the number of AO$_3$ mixed layers in each perovskite slab is n and that of occupied B layers is $(n - 1)$ [7–10].

---

[1] Present address: ITM Power PLC, Unit H, Sheffield Airport Business Park, Europa Link, Sheffield S9 1XU, UK.
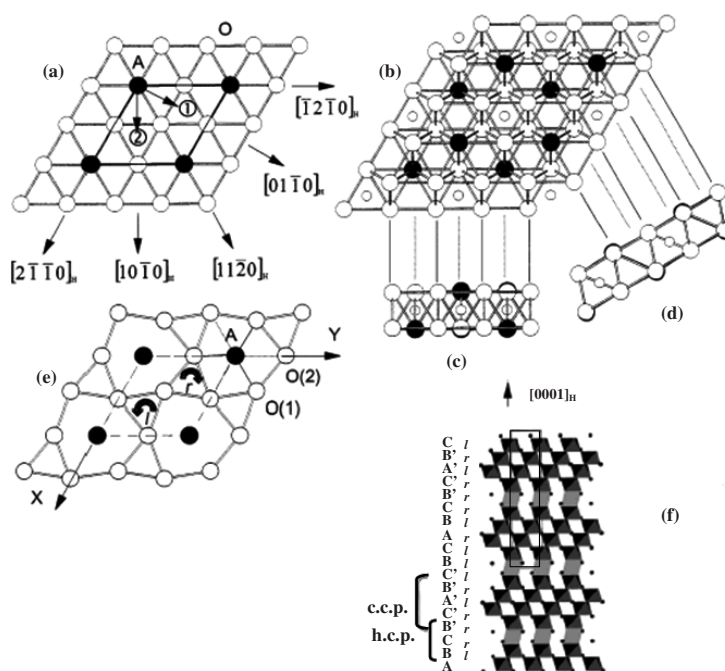
Figure 1. Schematic views of the AO_3 mixed layers packing in BLT: (a) arrangement of A and O atoms in the AO_3 mixed layers; (b) stacking of two adjacent AO_3 layers, showing the TiO_6 octahedra; (c) view of this stacking along $[10\bar{1}0]_H$; (d) view of this stacking along the $[11\bar{2}0]_H$ direction; (e) the distorted AO_3 layers in BLT–*r* and *l* visualize the clockwise and counterclockwise rotations of corner-sharing octahedral respectively; (f) schematic representation of BLT as viewed along $[2\bar{1}\bar{1}0]_H$, where the rotations of TiO_6 octahedra around the *c*-axis are represented by *r* (clockwise) and *l* (counterclockwise). ccp and hcp represent cubic close-packed and hexagonal close-packed, respectively.

Several recent structural studies have been devoted to the $A_n Ti_{n-1} O_{3n}$ compounds with $n = 5$ and A = Ba, La, i.e. $BaLa_4 Ti_4 O_{15}$ (BLT) [7–10]. It has been reported that the structure of BLT corresponds to close packing of AO_3 (where A = Ba, La) mixed layers. Within the layers, the A and O atoms are ordered; see figure 1(a). Each A atom is surrounded by six oxygen atoms, whereas each oxygen atom has two linearly coordinated A atoms among its six nearest neighbours. To avoid any direct A–A connection, successive layers are shifted from each other by a $1/3\langle 01\bar{1}0\rangle_H$ vector, so that the A atom positions in one layer project into the centre of a triangle formed by the A atoms in the adjacent layers (position 1 or 2 in figure 1(a)). One quarter of the octahedral interstices between two such layers are surrounded exclusively by oxygen atoms and are occupied by Ti atoms (the small open circles in figures 1(b)–(d)). All oxygen octahedra located within the cubic-close-packed (ccp) part of the sequence are corner-sharing and occupied by Ti atoms. In each triplet of face-sharing octahedra, characteristic of the hexagonal-close-packed (hcp) part of the sequence, the central octahedra are vacant. The lattice parameter *a* is determined by the hexagonal sublattice of A atoms and remains nearly constant at ∼5.6 Å. The *c* parameter depends on the stacking sequence of AO_3 layers (the thickness of each octahedral sheet is ∼2.2 Å). In the case of BLT, $n = 5$, and a cooperative tilting of TiO_6 octahedra within the perovskite blocks leads to doubling of the *c*-axis. As a consequence, BLT is ascribed as a trigonal structure with the space group $P\bar{3}c1$, and the lattice parameters derived

from x-ray diffraction data are $a = 5.5720$ Å and $c = 22.500$ Å ($\approx 10 \times 2.2$ Å), respectively, in the hexagonal setting [7–10].

In BLT, the large anisotropy in lattice parameters ($a = 5.5720$ Å versus $c = 22.500$ Å) promotes the growth of lath or plate-like particles. Such grains have been reported to align during powder pressing with the a, b plane normal to the pressing direction, and the final sintered body is therefore grain-oriented, as reported for compounds with a similar plate-or lath-like grain structure, e.g. $SrBi_4Ti_4O_{15}$ [11], $PbBi_4Ti_4O_{15}$ [12], and $Ba_{6-3x}Ln_{8+2x}Ti_{18}O_{54}$ [13]. This inevitably leads to anisotropy in various electric properties [12–17]. However, compared to $Ba_{6-3x}Ln_{8+2x}Ti_{18}O_{54}$ [1–3, 13], reports on BLT are rare and have only concentrated on x-ray diffraction data of BLT powders or single crystals [7–10]. Very few studies have been carried out on sintered ceramics and even fewer have considered their dielectric properties. In this paper, the crystal structure and microstructure of BLT sintered ceramics are investigated using x-ray diffraction (XRD), scanning and transmission electron microscopy (SEM and TEM) and Raman spectroscopy. Their dielectric properties at microwave frequencies are also evaluated.

2. Experimental details

Ceramics were synthesised by a conventional mixed oxide route using $BaCO_3$, TiO_2, and La_2O_3. The chemical purity of all these raw starting materials was $>99\%$. The weighed starting reagents in appropriate ratios were milled in distilled water in a high-energy attrition mill (a Szegvari Attritor System, from Union Process, OH, USA) for 1 h, using zirconia media. The slurry was dried, sieved and then calcined for 6 h at 1250 °C. Calcined powder was re-milled, sieved and then pressed into discs. Discs were sintered at 1450 °C for 6 h on zirconia boards. All of the fired samples have relative densities above 96%.

An x-ray diffractometer (Model PW 1730/10 from Philips, The Netherlands) with a Cu Kα source ($\lambda = 1.540\,562$ Å), operated at 40 kV and 30 mA, was used for the identification of phases and the evaluation of grain orientations. A step size of 0.02°, a scan rate of 1° min^{-1}, and scan ranges of 10–60° were adopted. The polished surfaces of sintered BLT ceramics were examined by XRD in both planar section (surface plane of the sample is parallel to the pressing direction) and cross section (surface plane of the sample is perpendicular to the pressing direction).

High-resolution powder XRD data for Rietveld structural refinement were collected using a Stoe STADI-P diffractometer in transmission mode, with a small linear position-sensitive detector (PSD), a Ge monochromator and Co Kα radiation. Data were collected over a $5 \leqslant 2\theta \leqslant 100°$ range, a step-width of 0.1° and a count time 45 s, and patterns were indexed using Stoe software packages.

Polished ceramics for SEM were prepared in both planar sections and cross sections and thermally etched and then coated with carbon before SEM examination. A Camscan SEM (Series II, Cambridge, UK) equipped with energy-dispersive spectroscopy (EDS), operating at 20 kV, was used to image the grain structures of the samples.

For TEM, BLT sintered ceramic pieces in planar section were ground flat on one side using a Gatan disc grinder stub. The ceramic was then removed from the Gatan disc grinder stub and remounted with the flat side down. The sample was further ground to approximately 20 μm thick and a 3.05 mm Cu support ring with a 800 μm circular hole was glued onto its surface using an epoxy resin. The sample was removed from the stub and excess Crystalbond was cleaned off its surface using acetone. The samples were then thinned in a Gatan Duo Mill ion beam thinner operating at an accelerating voltage of 6 kV and a combined gun current of 0.6 mA at an incidence angle of 12°. The samples were examined using an FEI Tecnai 20 TEM operating at an accelerating voltage of 200 kV and equipped with EDS.

A Renishaw inVia Raman microscope was used for Raman measurements. This system comprised an integral Raman microscope, a stigmatic single spectrograph, and a Peltier-cooled CCD detector, and the excitation wavelength used was 514 nm. A power of 20 mW was incident on the samples in a 1–2 μm diameter spot through a standard 50× microscope objective lens. The spectra were collected with a 30 s data-point acquisition time, a spectral range of 150–950 cm^{-1} and a spectral resolution of $\sim$2 cm^{-1}. Raman data were then analysed using WiRE$^{\text{TM}}$ 2.0, which is a fully interactive data processing package including peak fitting, data smoothing, quantitative analysis, peak picking, and integration for Raman spectrum analysis. Spectra were presented as relative intensity (counts) versus Raman shift (wavenumber cm^{-1} in air).

The low-frequency (1 kHz–10 MHz) ε_r was measured using an HP4192A impedance analyser. In order to examine the anisotropic nature of this material, samples for low-frequency ε_r measurements were electroded with silver in two ways: in one of them, the electric field is applied parallel [∥] to the pressing axis (i.e. planar-section sample); in the other, the electric field is perpendicular [⊥] to the pressing axis (i.e. cross-section sample).

Microwave measurements (ε_r, Q and τ_f) were performed using a silver-plated aluminium cavity and an Agilent 8753ES vector network analyser with a range of 30 kHz–6 GHz. Sintered samples in planar section were located at the centre of the cavity on an alumina support. The microwave energy was coupled to the test piece using a single probe, measuring in reflectance. After calibration for the cables and cavity, the coupling was adjusted such that losses were lower than −30 dB. Q is approximated using equation (1),

$$Q = f_0/BW \tag{1}$$

where f_0 is the resonant frequency and BW is the bandwidth measured at 7 dB from the resonant peak minimum. τ_f measurements were performed in the same aluminium cavity placed inside a Tenney temperature control cabinet. Resonant frequency measurements were performed at 80, 20 and −20 °C. τ_f was then calculated using equation (2),

$$\tau_f = (f_{80} - f_{-20})/(f_{20} \times 100) \tag{2}$$

where f_{80} is the resonant frequency at 80 °C, f_{-20} is the resonant frequency at −20 °C, and f_{20} is the resonant frequency at 20 °C.

3. Results and discussion

3.1. Crystal structure determined by XRD

Figure 2 shows an XRD trace obtained from BLT powder calcined at 1250 °C for 6 h. All peaks may be indexed according to a trigonal structure with a space group of $P\bar{3}c1$ and lattice parameters in the hexagonal (H) setting, $a_{\text{H}} = 5.57$ Å and $c_{\text{H}} = 22.48$ Å, which generally agree with those reported [7–10]. However, on careful examination of the peak profiles, weak asymmetry is observed on reflections such as (10$\bar{1}$2), (10$\bar{1}$4), (11$\bar{2}$0), (20$\bar{2}$6). In order to further study the asymmetry, higher-resolution XRD data were obtained from several high-order peaks at large 2θ angles. Figures 3(a)–(c) show expanded regions around the (11$\bar{2}$10), (02$\bar{2}$12) and (03$\bar{3}$10) peaks. Each shows a small degree of asymmetry. Representing the hexagonal $P\bar{3}c1$ cell in a monoclinic subgroup, which allows the three-fold symmetry to be broken while retaining one of the c-glide planes, results in a cell with $C2/c$ symmetry. XRD data were refined in both the $P\bar{3}c1$ ($a = 5.569\,95$ Å, $c = 22.4779$ Å) and $C2/c$ ($a = 9.6470$ Å, $\beta = 5.5702$ Å, $c = 22.4778$ Å, $b = 89.95°$) cells for comparison and, although the monoclinic settings gave a marginally superior fit, the c^2, R_{wp} and R_{p} values were statistically equivalent, as indicated in table 1. However, another plausible explanation for asymmetry in the high-order
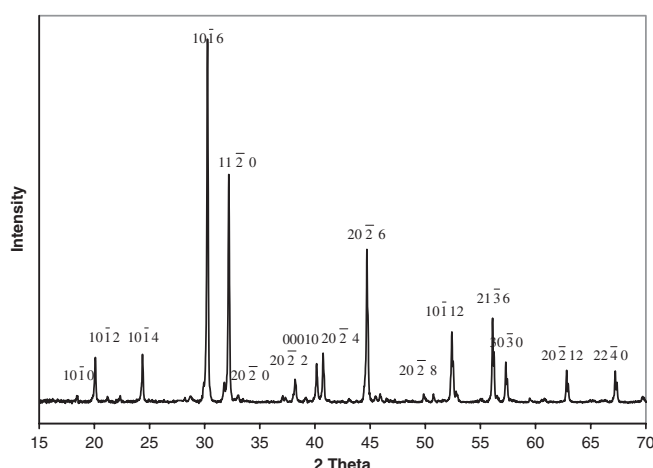
Figure 2. XRD trace obtained from BLT powder calcined at 1250 °C and indexed according to $P\bar{3}c1$ cell with $a = 5.569\,95$ Å and $c = 22.4779$ Å in accordance with [7–10].

Table 1. Rietveld structural refinement data for BLT.

Unit cell: hexagonal		Unit cell: monoclinic	
Space group: $P\bar{3}c1$		Space group: $C2/c$	
$a = 5.57$ Å, $c = 22.48$ Å		$a = 9.6407$ Å, $b = 5.5702$ Å, $c = 22.4778$ Å, $\beta = 89.95°$	
χ^2	1.205	χ^2	1.174
R_{wp}	3.67%	R_{wp}	3.62%
R_p	2.79%	R_p	2.78%
Variables	31	Variables	48

XRD peaks obtained from BLT may be that two hexagonal phases with slightly different lattice parameters coexist in BLT sintered ceramics. In order to further investigate the structure and composition of BLT, electron diffraction and energy-dispersive x-ray analysis were carried out.

3.2. Electron diffraction and energy-dispersive x-ray spectroscopy

As discussed above, the structure of BLT has previously been described as trigonal, $P\bar{3}c1$, with lattice parameters in the hexagonal (H) setting $a_H \approx 5.57$ Å and $c_H \approx 22.5$ Å. Figures 4(a), (b) and (c) are [0001], [$\bar{1}$100] and [1$\bar{2}$10] zone axes, indexed according to the above hexagonal setting [7–10]. The reflection conditions for the $P\bar{3}c1$ space group allow only {000l} reflections where $l = 2n$. However, in the [$\bar{1}$100] zone axis (figure 4(b)), double diffraction gives rise to the {000l} where $l = 2n+1$. Hence, the [$\bar{1}$100] zone may be used to directly measure the c-axis parameter, $d_{0001} \sim 23$ Å, confirming that the structure has $n = 5$. The more intense reflections in the patterns correspond to $\sim d_{(111)}$ of the cubic-close-packed AO$_3$ perovskite lattice. There is no significant deviation from 60° between the {$\bar{1}$010} reflections in figures 4(a)–(c), which show that only the expected 90° angles between planes normal to (0001), thereby confirming that any monoclinic distortion is slight.

In order to assess the compositional distribution of the ions throughout the BLT ceramics, EDS analyses were performed on 20–30 randomly chosen grains. In general, two sets of characteristic EDS spectra were obtained, as shown in figures 5(a) and (b). Both spectra confirm
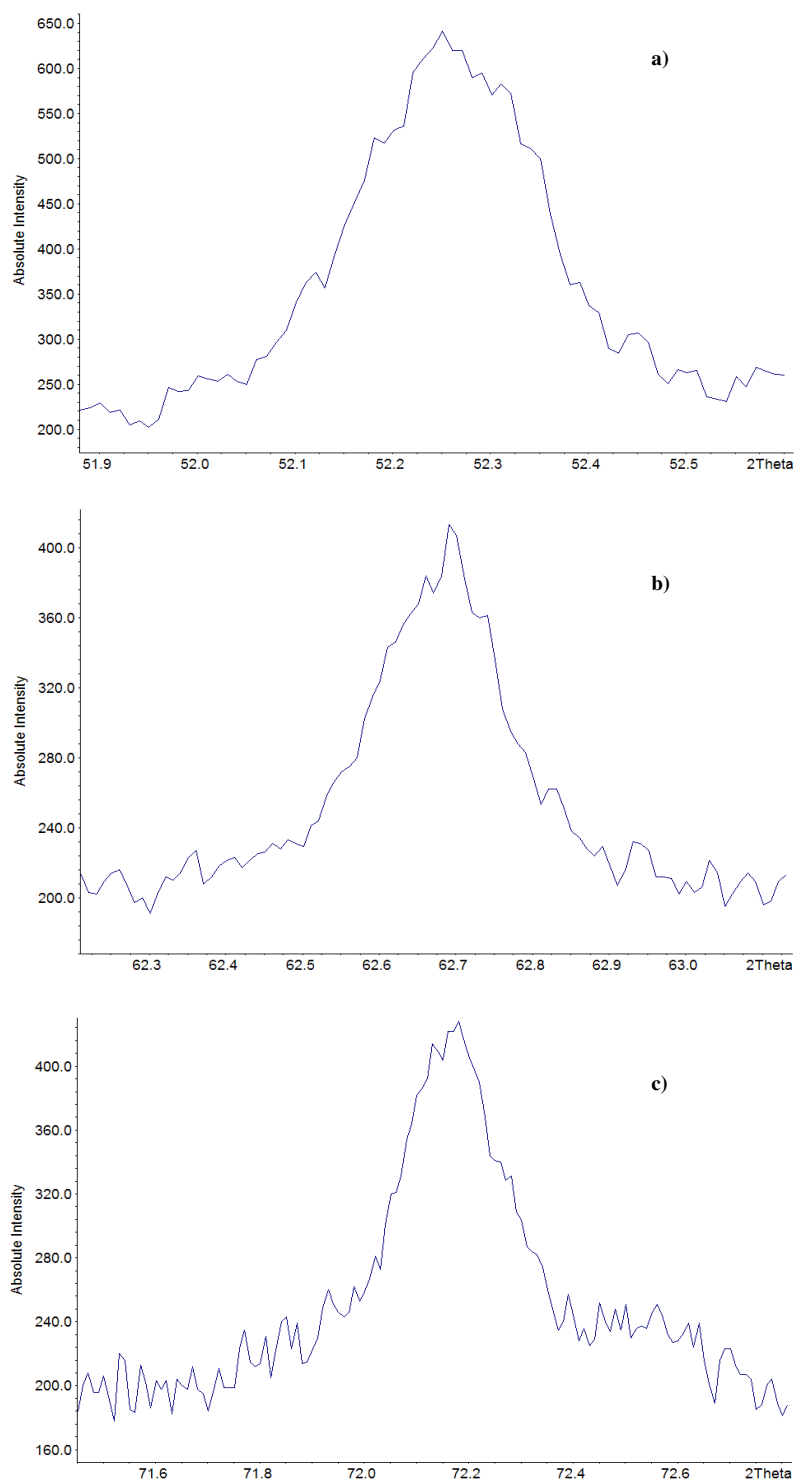
Figure 3. Peak asymmetry/splitting observed on peaks (a) $(11\bar{2}10)$, (b) $(02\bar{2}12)$, and (c) $(03\bar{3}10)$. (This figure is in colour only in the electronic version)
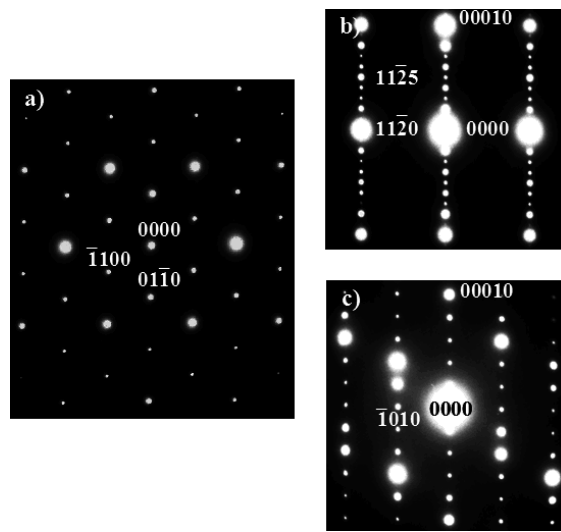
Figure 4. (a)–(c) [0001], [$\bar{1}$100] and [1$\bar{2}$10] zone axes from grains in BLT indexed according to the hexagonal cell a ≈5.57 Å and $c \approx 22.5$ Å reported in [7–10].
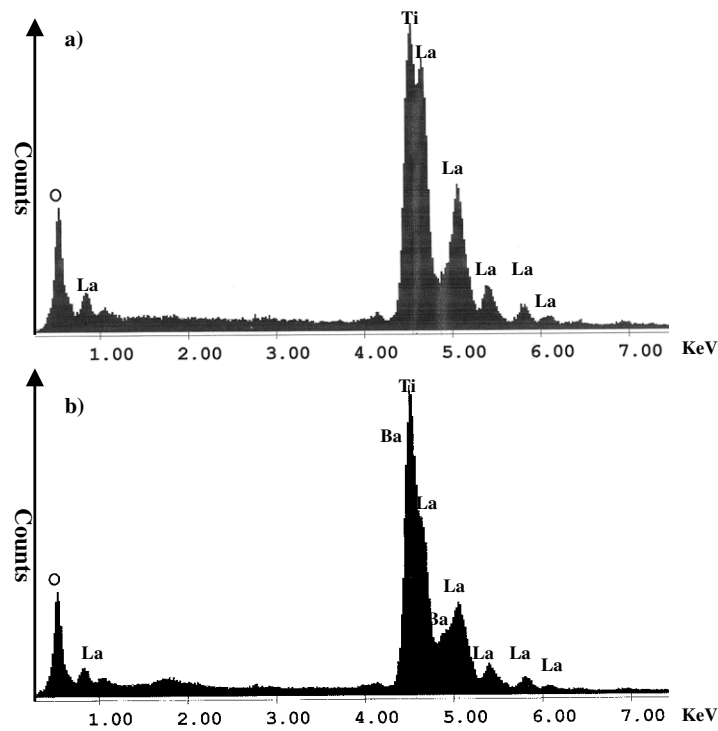

Figure 5. (a) and (b) Typical EDS spectra obtained from several grains in BLT ceramics.

the presence of La, Ti, Ba, and O in BLT. No other element is detected. The strong overlap of peaks associated with Ba, Ti and La means that fully quantitative analysis is very difficult to
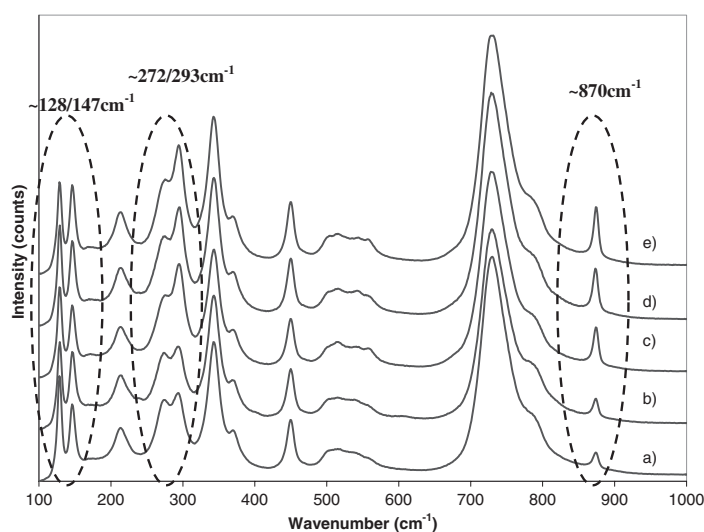
Figure 6. Raman spectra obtained from different grains (a)–(e) in BLT ceramics.

achieve, since extensive and complex de-convolution techniques are necessary to obtain reliable data. Here, however, the same quantification programmes and sub-routines were used on each spectrum and the results are comparative rather than absolute. In particular, the La/Ti ratio (1:1 in the stoichiometric formula unit) is clearly different for figure 5(a) (1.4) compared with figure 5(b) (0.83). Irrespective of the difficulties of de-convoluting La, Ti and Ba peaks in the EDS spectroscopy, such strong differences in the La/Ti ratio may only be explained by considering that there is an intergranular, heterogeneous distribution of the constituent cations. The observation of two different sets of EDS spectra associated with sintered BLT ceramics suggests that the simplest explanation for asymmetry in high-order XRD peaks (figures 3(a)–(c)) is the presence of two hexagonal phases with marginally different lattice parameters. In order to further investigate the grain-to-grain variation in composition and/or structure, micro-Raman spectroscopy was performed.

3.3. Raman spectroscopy

Figures 6(a)–(e) show the Raman spectra obtained from different grains, **a–e**, in BLT sintered ceramics. The positions of all the peaks in these spectra are identical, suggesting that only modes associated with the same (hexagonal) phase of BLT are present. However, different intensity profiles are observed, as typified by the modes at $\sim$870 cm^{-1} and the doublets at $\sim$128/147 cm^{-1} and $\sim$272/293 cm^{-1}. Similar to $Ba_5Nb_4O_{15}$ [17–19] and $Ba_5Ta_4O_{15}$ [20], Raman peaks located at $\sim$128 cm^{-1}/147 cm^{-1} may be assigned to the motion of A-site cations (Ba/La) respectively. Though the positions of these two peaks are almost identical in each trace, their relative intensity changes in different grains, figures 6(a)–(e), implying that the A-site cation (Ba/La) distribution may not be homogeneous, which agrees well with the EDS data (figure 5).

Usually, the occurrence of Raman peaks at $\sim$870 cm^{-1}, the so-called oxygen breathing A_{1g} mode in complex perovskites, may be attributed to the presence of different cations on the B-site, corresponding to the vibration of the oxygen octahedral cage. In BLT, there are B-site vacancies which, in principle, are associated with face-shared octahedra in the structure.
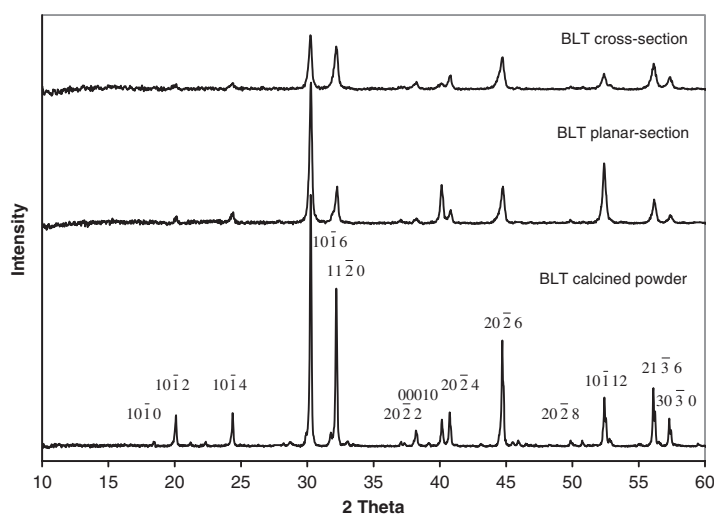
Figure 7. XRD traces from (a) BLT powder calcined at 1250 °C and ceramics sintered at 1450 °C for 6 h and examined in (b) planar section and (c) cross section.

However, a variation in the cation concentration may well create a distribution of B-site vacancies from grain to grain and modify the intensity of this peak.

Although the assignments of the peaks and the interpretation of their intensity is speculative, there is no doubt that the spectra differ from grain to grain, supporting the EDS data, which demonstrates a heterogeneous distribution of cations. It is reasonable to conclude therefore from the XRD, EDS and Raman data that two different hexagonal unit cells are present in BLT, each with marginally different lattice parameters.

3.4. Microstructure and anisotropy

Figure 7 shows XRD traces from (a) BLT powder calcined at 1250 °C and ceramics sintered at 1450 °C for 6 h and examined in (b) planar section and (c) cross section. In order to quantify any preferred orientation, it is assumed that the calcined BLT powder (figure 7(a)) is essentially randomly oriented and therefore the resulting XRD trace may be used as a reference. The ratio (R) of the intensity of the (0001) plane (perpendicular to the c-axis) to the (11$\bar{2}$0) plane (parallel to the c-axis) in a BLT powder sample is approximately 0.17; figure 7(a). This ratio R increases considerably to ~1.08 in the trace of the sintered BLT ceramic, figure 7(b), indicating a higher percentage of (0001) planes normal to the pressing direction and a strong c-axis orientation along the pressing direction. In contrast, the R ratio of the BLT ceramic examined parallel to the pressing axis, figure 7(c), is ~0.13, which is lower than the value obtained from the powder sample. This demonstrates that the a, b plane in the cross-section sample (equivalent to the c plane in the planar-section sample) is preferentially oriented parallel to the pressing direction.

Figures 8(a)–(c) are secondary-electron SEM images taken from (a) BLT powder, and BLT ceramic examined (b) in planar section (the surface of the plane is parallel to the pressing direction) and (c) cross section (the surface of the plane is normal to the pressing direction). The BLT powders reveal characteristic platelet particles [11, 14, 16], a morphology which is retained in the sintered ceramic. Figures 8(b) and (c) reveal that no second phases are present in the sintered ceramics. However, compared to the powder sample, the grains are further
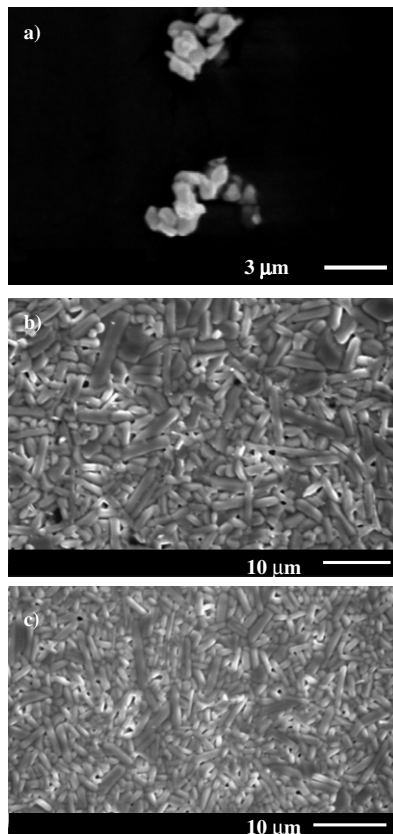
Figure 8. Secondary-electron SEM images taken from (a) BLT powder, and BLT ceramic examined in (b) planar section (the surface plane of the sample is parallel to pressing direction) and (c) cross section (the surface plane of the sample is normal to the pressing direction).

elongated, and the aspect ratio of the plate-shaped grains ranges from 3 to 6. If figures 8(b) and (c) are compared, it is evident that there is some alignment of the platelets in figure 8(c) (cross-section sample) but that the distribution of the laths is more random in figure 8(b) (planar-section sample). This indicates that most of the grains (*c*-axis) align along with the pressing direction, confirming the anisotropic grain growth in BLT sintered ceramics due to the ceramic pressing process.

Figure 9 shows a bright-field (BF) image taken from planar-sectioned BLT ceramics. Planar defects are observed in most grains. There was no attempt to control the orientation of the sample in order to study the planar defects systematically. However, their morphology is consistent with stacking faults which have been reported previously in hexagonal perovskites.

3.5. Dielectric properties

Figure 10 is a plot of ε_r versus log frequency (f) of BLT ceramics measured in planar section and cross section. $\varepsilon_r[\perp]$ (the applied electric field perpendicular to the pressing direction, i.e. cross-section sample) was 52, whereas $\varepsilon_r[\parallel]$ (the applied electric field parallel to the pressing direction) was only 42. The ∼20% difference between $\varepsilon_r[\parallel]$ and $\varepsilon_r[\perp]$ clearly demonstrates anisotropic dielectric behaviours which can only be related to the anisotropy of
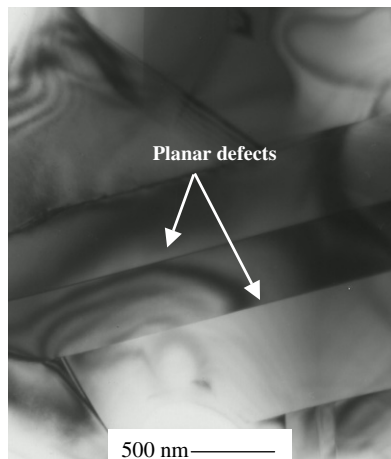
Figure 9. Bright-field (BF) TEM image taken from a planar section of a BLT ceramic, showing planar defects in non-specific orientation.
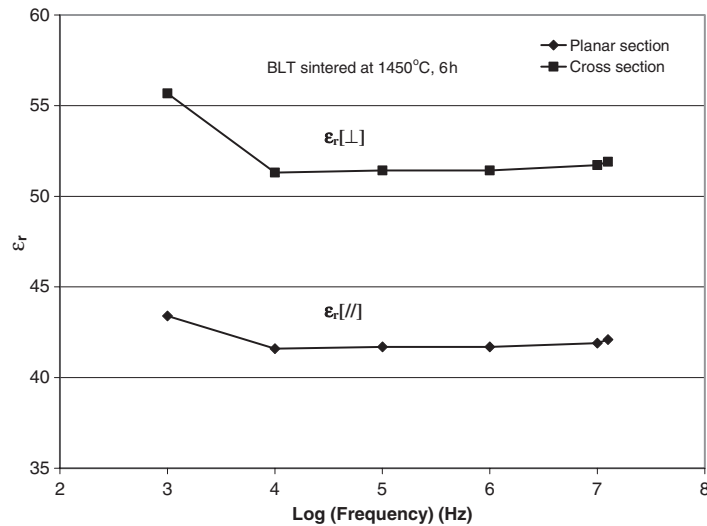

Figure 10. Plot of ε_r versus log frequency (f) of BLT ceramics measured in planar and cross section.

grain orientation induced by the ceramic processing. No anisotropy of dielectric properties has been reported in single-crystal data of BLT, but it is likely to be present. Similar behaviour has also been observed for other compounds which are known to form lath-or plate-like particles, such as Bi$_4$Ti$_3$O$_{12}$ [14], PbBi$_4$Ti$_4$O$_{15}$ [15] and Pb$_2$Bi$_4$Ti$_5$O$_{18}$ [15]. There is a clear potential in BLT ceramics to further enhance the grain orientation, thereby exaggerating the anisotropy of the dielectric properties at rf frequencies. Several methods may be used to achieve highly orientated ceramics such as hot-pressing [16], hot-forging [11, 12, 14] or tape-casting combined with templated grain growth (TGG) [13, 21].

Microwave frequency measurements were carried out in a conventional cavity, nominally on a planar section. An ε_r of ~45, Qf values as high as ~43 589 GHz (@4 GHz) and a

near-zero τ_f of -2 ppm $°C^{-1}$ were obtained. These values are compatible or superior to those reported in the literature [4, 5]. It is not known, however, whether it is possible to observe the same anisotropy of the dielectric properties in microwave measurements as observed at lower frequencies. The interaction of the electromagnetic field with the ceramic is not unidirectional at rf frequencies and may average out the dielectric response.

4. Conclusions

- A weak asymmetry is reported for appropriate high-order peaks in XRD data for BLT ceramics.
- EDS revealed a strong variation in the La:Ti ratio from grain to grain, which implies a heterogeneous distribution of the constituent cations.
- Raman spectroscopy data from several grains exhibit the same modes but often with different relative intensities, which further suggests a heterogeneous distribution of cations.
- It is concluded therefore that the asymmetry observed in XRD data occurs as a result of the presence of two different hexagonal phases with different compositions and therefore marginally different lattice parameters.
- Grain orientation during ceramic processing results in anisotropy of the relative permittivity, measured at rf frequencies.
- Microwave measurements confirmed that BLT ceramics have $Q\sim44\,000$ GHz, $\varepsilon_r = 45$, and a near-zero τ_f (-2 ppm $°C^{-1}$).

References

[1] Jaakola T, Uusimäki A, Rautioaho R and Leppävuori S 1986 *J. Am. Ceram. Soc.* **69** C234–5
[2] Wakino K, Minai K and Tamura H 1984 *J. Am. Ceram. Soc.* **67** 278–81
[3] Ohsato H and Imaeda M 2003 *Mater. Chem. Phys.* **79** 208–12
[4] Vineis C, Davies P K, Negas T and Bell S 1996 *Mater. Res. Bull.* **31** 431–7
[5] Okawa T, Kiuchi K, Okabe H and Ohsato H 2001 *Japan. J. Appl. Phys.* **40** 5779–82
[6] Lander J J 1951 *Acta Crystallogr.* **4** 148–56
[7] Harre N, Mercurio D, Trolliard G and Frit B 1998 *Mater. Res. Bull.* **33** 1537–48
[8] Teneze N, Mercurio D, Trolliard G and Frit B 2000 *Mater. Res. Bull.* **35** 1603–14
[9] Trolliard G, Harre N, Mercurio D and Frit B 1999 *J. Solid State Chem.* **145** 678–93
[10] Harre N, Mercurio D, Trolliard G and Mercurio J P 1998 *Ann. Chim. Sci. Mater.* **23** 233–6
[11] Gelfuso M V, Thomazini D and Eiras J A 1999 *J. Am. Ceram. Soc.* **82** 2368–72
[12] Takenaka T and Sakata K 1984 *J. Appl. Phys.* **55** 1092–9
[13] Wada K, Kakimoto K I and Ohsato H 2003 *Japan. J. Appl. Phys.* **42** 6149–53
[14] Takenaka T and Sakata K 1980 *Japan. J. Appl. Phys.* **19** 31–9
[15] Miyayama M and Yi I S 2000 *Ceram. Int.* **26** 529–33
[16] Zhang Z, Yan H, Xiang P, Dong X and Wang Y 2004 *J. Am. Ceram. Soc.* **87** 602–5
[17] Ratheesh R, Sreemoolanadhan H and Sebastian M T 1997 *J. Solid State Chem.* **131** 2–8
[18] Zhao H, Feng S, Xu W, Shi Y, Mao Y and Zhu X 2000 *J. Mater. Chem.* **10** 965–8
[19] Massa N E, Pagola S and Carbonio R 1996 *Phys. Rev.* B **53** 8148–50
[20] Abakumov A M, Shpanchenko R V and Antipov E V 1998 *J. Solid State Chem.* **141** 492–9
[21] Duran C, Trolier-McKinstry S and Messing G L 2000 *J. Am. Ceram. Soc.* **83** 2203–13